

Simulation of Thermal Relaxation in Spin Chemistry Systems on a Quantum Computer Using Inherent Qubit Decoherence

Brian Rost,^{1,2} Barbara Jones,¹ Mariya Vyushkova,³ Aaila Ali,^{1,4,5}
Charlotte Cullip,^{1,6} Alexander Vyushkov,³ and Jarek Nabrzyski³

¹*IBM Research - Almaden, 95120 San Jose, CA*

²*Department of Physics, Georgetown University, 20057 Washington, DC*

³*Center for Research Computing, University of Notre Dame, 46556 Notre Dame, IN*

⁴*Department of Physics, DePaul University, 60614 Chicago, IL*

⁵*Department of Computer Engineering, Illinois Institute of Technology, 60616 Chicago, IL*

⁶*Departments of Chemistry and Computer Science, Occidental College, 90041 Los Angeles, CA*

(Dated: November 10, 2020)

Current and near term quantum computers (i.e. NISQ devices) are limited in their computational power in part due to qubit decoherence. Here we seek to take advantage of qubit decoherence as a resource in simulating the behavior of real world quantum systems, which are always subject to decoherence, with no additional computational overhead. As a first step toward this goal we simulate the thermal relaxation of quantum beats in radical ion pairs (RPs) on a quantum computer as a proof of concept of the method. We present three methods for implementing the thermal relaxation, one which explicitly applies the relaxation Kraus operators, one which combines results from two separate circuits in a classical post-processing step, and one which relies on leveraging the inherent decoherence of the qubits themselves. We use our methods to simulate two real world systems and find excellent agreement between our results, experimental data, and the theoretical prediction.

I. INTRODUCTION

As spin 1/2 particles are “nature’s qubits” (simple two-state systems), electron spins map onto quantum devices in a straightforward, natural way. Because of that, it is interesting to focus on quantum applications of chemistry problems involving electron spin dynamics, such as spin chemistry simulations. Spin chemistry is an interdisciplinary subfield of physics and chemistry dealing with magnetic and spin effects in chemical reactions, which connect quantum phenomena like superposition and entanglement directly to macroscopic, measurable chemical parameters such as reaction yields, and make it possible to dynamically visualize those phenomena in chemistry experiments.

Historically, the fields of spin chemistry and quantum information science are closely related. On the one hand, spin chemistry expertise has contributed significantly to development of quantum computation, especially to spin-based qubit implementations[1–9]. At the same time, novel and promising approaches to spin chemistry problems (most prominently, avian magnetoreception mechanism), originating from the quantum information science field, have recently been introduced[10–23].

Among spin chemistry problems, we have identified a simple yet experimentally important model simulation problem - quantum beats in radiation-generated radical pairs[24–27]. In a typical experiment, a burst of ionizing radiation is sent through a solution, forming radical pairs in a spin-correlated singlet state, due to spin conservation in the ionization process. This state then evolves due to hyperfine couplings (HFC), unequal Larmor precession rates (caused by unequal g -factors) in the presence of a magnetic field, and paramagnetic relaxation[24–28]. The

radical pairs undergo spin-selective recombination reactions, resulting in a fluorescent product when recombining in the singlet state, but not when recombining in a triplet state. The dynamics of the spin state of the radical pairs, often called “quantum beats”, offers insights into the properties of the pairs’ constituent molecules, allowing for determination of e.g. g -factors and HFC constants. Recently, a new theoretical approach treating spin-selective recombination of radical pairs as a quantum measurement that collapses the wavefunction into one of the total spin eigenstates (either singlet or triplet), has been suggested and actively discussed [10, 13, 17, 29–39]. Therefore, the radical pair simulation problem can be described as time evolution of qubit pairs initialized in an entangled state [4, 6, 7], where spin-selective recombination plays a role of quantum measurement, which makes the radical pair mechanism a very interesting and promising application for quantum simulation.

The intensity of the observed fluorescence is approximately given by[24, 28]

$$I(t) = F(t) \left(\theta S(t) + \frac{1}{4}(1 - \theta) \right) \quad (1)$$

where $F(t)$ is the time-dependent radical pair recombination rate, θ is the experimentally determined fraction of recombination events occurring between RPs produced from the same precursor and $S(t)$ is the probability of a RP being in the singlet state, which generally depends on magnetic field strength B . The spin dynamics are extracted from the fluorescence profile using the time-resolved magnetic field effect (TR-MFE) method. This is done by taking a ratio of $I(t)$ at high-field and low-field to cancel $F(t)$, which has no B dependence. A quantity, Q , subject to a high-field is denoted as Q_B and subject

to a low-field as Q_0 . Using Eq. 1 we have for the TR MFE

$$M(t) = \frac{I_B(t)}{I_0(t)} = \frac{F(t)}{F'(t)} \left(\frac{4\theta S_B(t) + (1-\theta)}{4\theta S_0(t) + (1-\theta)} \right). \quad (2)$$

In this paper we present two methods for computing various quantities of interest, subject to thermal relaxation, on currently available quantum computers. A quantity, Q , calculated for an isolated system is denoted as \tilde{Q} when subject to thermal relaxation.

In section II we cover the relevant theory of spin chemistry and thermal relaxation, as well as introducing the two real world systems we use to test our algorithms. In section III we present our algorithms for simulating thermal relaxation in these systems and discuss their scope and scalability. In section IV we present data taken from applying our algorithms to these systems on real quantum computers provided by IBMQ[40].

II. THEORY

A. Calculation of $S(t)$

We consider systems of radical pairs in non-viscous solutions with no exchange between the pair's constituents. Such systems are described by Hamiltonians of the form[24, 26, 41, 42]

$$H = \sum_{i=1}^2 \left[\mu_B g_i \mathbf{B} + \sum_{j=1}^{N_i} a_{ij} \mathbf{I}_{ij} \right] \cdot \mathbf{S}_i. \quad (3)$$

Here μ_B is the Bohr magneton, \mathbf{S}_i (g_i) is the spin (g -factor) of the unpaired electron in molecule i , \mathbf{I}_{ij} refers to the j^{th} nuclear spin in molecule i , a_{ij} is the HFC constant between \mathbf{S}_i and \mathbf{I}_{ij} , and \mathbf{B} is the magnetic field.

From this Hamiltonian, we seek an expression for $S(t)$, the probability of a pair being in the singlet state at time t , given it was initially created in the singlet state at time $t = 0$. Alternatively, $S(t)$ may be thought of as the fraction of pairs, which were initially in the singlet state, found in the singlet state at time t . While the initial electronic state of the pair preserves the spin multiplicity of its precursor[26], the initial nuclear state has no constraints. Therefore, following Brocklehurst[27], we take the initial nuclear state of a newly formed RP to be the maximally mixed state (i.e. all nuclear states are equally likely). This gives an initial state of

$$\rho(0) = \frac{1}{N_{\mathbf{I}}} |S\rangle\langle S| \otimes I_{N_{\mathbf{I}}} \quad \text{with} \quad |S\rangle = \frac{|01\rangle - |10\rangle}{\sqrt{2}}. \quad (4)$$

where I_n is the $n \times n$ identity matrix and $N_{\mathbf{I}}$ is the size of the Hilbert space of the nuclear spins.

We then compute $S(t)$ by evolving $\rho(0)$ by time t under the H from Eq. 3, tracing out the nuclear degrees of

freedom (DOF) and taking the expectation value of the resulting reduced electronic density matrix w.r.t. $|S\rangle$

$$S(t) = \langle S | \text{Tr}_{\mathbf{I}} \{ e^{-iHt} \rho(0) e^{iHt} \} | S \rangle. \quad (5)$$

There is no analytic expression for Eq. 5 in general, although it is known for a variety of simple cases[24, 27, 39]. Evaluating Eq. 5 numerically is straightforward, however it becomes exponentially expensive in the number of nuclear DOFs.

B. Thermal Relaxation

The main mechanisms of relaxation in these systems are generalized amplitude damping (i.e. longitudinal paramagnetic relaxation or T_1 decay) and dephasing (i.e. transverse paramagnetic relaxation or T_2 decay)[24, 26, 27, 42–44]. It can be shown that only the effective T_1 and T_2 for the pair are relevant to $\tilde{S}(t)$ so for simplicity we take T_1 and T_2 to be equal for both radicals. The following remains unchanged if T_1 and T_2 are different for each radical. In general, we have $T^{-1} = T_a^{-1} + T_c^{-1}$ [43] where a and c stand for anion and cation respectively.

We derive an expression for the evolution of the singlet state probability, $\tilde{S}(t)$, subject to these decoherence channels, in terms of the singlet state probability for the isolated system, $S(t)$. In general, a proper description of the dynamics of a system undergoing both relaxation and coherent time evolution is very complicated because the relaxation channels and coherent time evolution do not commute. However, this is not always the case, as we demonstrate in this work for spin chemistry systems at room temperature.

A quantum channel, \mathcal{E} , can be characterized by its Kraus operators, K_i , and performs the operation[45]

$$\mathcal{E}(\rho) = \sum_i K_i \rho K_i^\dagger. \quad (6)$$

The Kraus operators for the generalized amplitude damping channel, \mathcal{E}_x , are[46]:

$$\begin{aligned} K_0^x &= \sqrt{p_n} \begin{pmatrix} 1 & 0 \\ 0 & \sqrt{p_x} \end{pmatrix} = \sqrt{p_n} \left(\frac{I+Z}{2} + \sqrt{p_x} \frac{I-Z}{2} \right) \\ K_1^x &= \sqrt{p_n} \begin{pmatrix} 0 & \sqrt{p_x} \\ 0 & 0 \end{pmatrix} = \sqrt{p_n} \left(\frac{X+iY}{2} \right) \\ K_2^x &= \sqrt{p_n} \begin{pmatrix} \sqrt{p_x} & 0 \\ 0 & 1 \end{pmatrix} = \sqrt{p_n} \left(\frac{I-Z}{2} + \sqrt{p_x} \frac{I+Z}{2} \right) \\ K_3^x &= \sqrt{p_n} \begin{pmatrix} 0 & 0 \\ \sqrt{p_x} & 0 \end{pmatrix} = \sqrt{p_n} \left(\frac{X-iY}{2} \right) \end{aligned} \quad (7)$$

Where $p_n = (1 + e^{-\beta})^{-1}$ is the Fermi function which gives the equilibrium population of $|0\rangle$ as a function of

inverse temperature, β . p_n can be viewed as a temperature parameter controlling the ratio of damping of $|1\rangle$ and $|0\rangle$. p_x is the damping parameter, and $\bar{\alpha} \equiv 1 - \alpha$. $T = 0(\beta = \infty) \rightarrow p_n = 1$ and we recover the standard amplitude damping channel, only $|1\rangle \mapsto |0\rangle$ occurs, with probability p_x . $T = \infty(\beta = 0) \rightarrow p_n = 1/2$ so $|1\rangle \mapsto |0\rangle$ and $|0\rangle \mapsto |1\rangle$ both occur with probability $p_x/2$.

The dephasing channel, \mathcal{E}_z , is given by the Kraus operators

$$K_0^z = \sqrt{\bar{p}_z} I \quad K_1^z = \sqrt{p_z} Z \quad (8)$$

which intuitively reads, ‘‘With probability p_z apply Z otherwise do nothing’’.

It is shown in Appendix A that \mathcal{E}_x and \mathcal{E}_z commute. Define commuting quantum channels as any two quantum channels, \mathcal{E}_1 and \mathcal{E}_2 that satisfy

$$[\mathcal{E}_1, \mathcal{E}_2] = 0 \implies \mathcal{E}_1(\mathcal{E}_2(\cdot)) = \mathcal{E}_2(\mathcal{E}_1(\cdot)). \quad (9)$$

Denote $\mathcal{E}(\rho) \equiv \mathcal{E}_x(\mathcal{E}_z(\rho)) = \mathcal{E}_z(\mathcal{E}_x(\rho))$. It is also shown that for Hamiltonians of the form given in Eq. 3, the time evolution of the electronic subsystem commutes with \mathcal{E}^∞ , \mathcal{E} at infinite temperature.

This is useful because, to a very good approximation, room temperature is infinite temperature for spin chemistry systems. The energies associated with the Hamiltonian in Eq. 3 for even the larger B fields used in spin chemistry experiments are orders of magnitude smaller than $k_B T$ at room temperature.

Note that the time evolution of the electronic subsystem is not a unitary operation and is itself given by a quantum channel, \mathcal{E}_U , such that

$$\mathcal{E}_U(\rho) = \text{Tr}_{\mathbf{I}} \{ e^{-iHt} \rho e^{iHt} \} \quad (10)$$

We are thus able to compute $\tilde{S}(t)$ by applying \mathcal{E}^∞ and \mathcal{E}_U only once, instead of needing to use more complicated methods, e.g. time ordered products or Trotterization, precisely because these channel commute. To find the correct p_x and p_z to apply at time t , we apply \mathcal{E}^0 (\mathcal{E} at $T = 0$) to a generic ρ and equate it to the known iterative infinitesimal result[45].

$$\mathcal{E}^0(\rho) : \begin{cases} \rho_{11} \mapsto \bar{p}_x \rho_{11} = e^{-t/T_1} \rho_{11} \\ \rho_{10} \mapsto \sqrt{\bar{p}_x} (1 - 2p_z) \rho_{10} = e^{-t/T_2} \rho_{10} \end{cases} \quad (11)$$

which gives

$$p_x = 1 - e^{-\frac{t}{T_1}} \quad \text{and} \quad p_z = \frac{1}{2} \left(1 - e^{-t \left(\frac{1}{2T_1} + \frac{1}{T_2} \right)} \right). \quad (12)$$

Finally, $\tilde{S}(t)$ is computed as

$$\begin{aligned} \langle S | \mathcal{E}^\infty(\mathcal{E}_U(\rho(0))) | S \rangle &= \langle S | \text{Tr}_{\mathbf{I}} \{ \mathcal{E}^\infty(\rho(t)) \} | S \rangle = \\ &= \frac{1}{4} \left(1 + e^{-t/T_1} + e^{-t/T_2} (4S(t) - 2) \right) \end{aligned} \quad (13)$$

which agrees with Ref. 24. Although this result is already known, the algorithm given in the Sec. III A relies on the fact that \mathcal{E}^∞ and \mathcal{E}_U commute. To the best of our knowledge, this has not previously been shown.

III. ALGORITHMS

We present two approaches for simulating the dynamics of these types of spin systems undergoing thermal relaxation on a quantum computer, and discuss the advantages and disadvantages of each. Both methods require implementing time evolution under the action of the Hamiltonian in Eq. 3. A wide variety of algorithms already exist for this step[47–50]. The novel part in the approaches is the implementation of thermal relaxation.

Firstly, we explicitly simulate the generalized amplitude damping (Eq. 7) and dephasing channels (Eq. 8). This has the advantage of being highly controllable since we are able to implement decoherence with any parameters we wish. However, it has the disadvantage of requiring a larger and deeper circuit which makes it less reliable, and scalable on NISQ devices.

Secondly, we leverage the decoherence of the qubits themselves to model the decoherence of the real spin system. This has the advantage that it requires no additional gates or qubits, so the circuit remains small and simple and should scale well to larger systems. However, it has the disadvantage that we are not in control of the decoherence parameters. A further complication is that the protocol requires waiting for the qubits to relax, which can amplify errors due to miscalibration. An in-depth discussion follows.

A. Explicit Decay, Kraus Method

We can implement the Kraus operators given in Eq. 7 and 8 using the quantum circuit shown in Fig. 1, following the approaches given in 51 and 52. The five gates operating only on the bottom three qubits implement the generalized amplitude damping channel, \mathcal{E}_x , while the two gates involving the top qubit implement the dephasing channel, \mathcal{E}_z .

It is easy to make sense of this circuit by thinking of the standard amplitude damping channel as: ‘‘If the qubit is in $|1\rangle$, apply an X gate with probability p_x .’’, the temperature correction part (added to give the generalized amplitude damping channel) as: ‘‘with probability p_n apply X to the amplitude damping control line, i.e. damp $|0\rangle$ instead of $|1\rangle$,’’ and similarly, the dephasing channel as: ‘‘With probability p_z apply a Z gate.’’

The circuit in Fig. 1 can be optimized greatly. Both the ‘‘Temp’’ and ‘‘Dephase’’ parts of the circuit in Fig. 1 can be thought of as probabilistically implementing a gate (X and Z respectively). This means the rotation gate and controlled operation can be replaced by a probabilistic gate.

1) We can run the circuit with and without each gate (X or Z), with the gate operating where the target of the (now deleted) controlled operation was, then taking a weighted average over the results. The weights should be the probabilities of the (now deleted) rotation gate leaving the ancilla in $|1\rangle$, i.e. $w_{XZ} = \bar{p}_n p_z$, $w_Z = p_n p_z$,

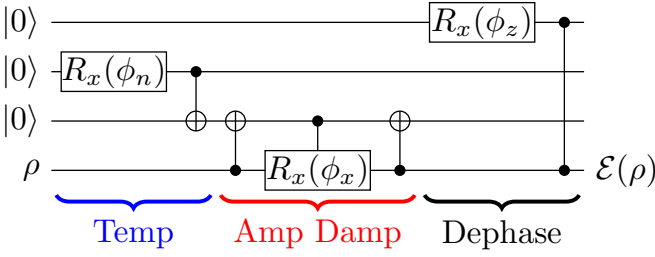


FIG. 1: Circuit to perform generalized amplitude damping, \mathcal{E}_x , and dephasing, \mathcal{E}_z , on a qubit. $\phi_{x,z} = 2 \sin^{-1}(\sqrt{p_{x,z}})$ and $\phi_n = 2 \cos^{-1}(\sqrt{p_n})$.

$w_X = \bar{p}_n \bar{p}_z$, $w_I = p_n \bar{p}_z$. Since the number of possible combinations grows exponentially as more qubits are added, this approach will not scale well. However, it is easy to implement using currently available quantum software and the systems under consideration here only have decoherence on the two electrons - making this our method of choice in this work.

2) Alternatively, we can run the circuit with an $R_x(\theta_n)$ and $R_z(\theta_z)$, with the gate operating where the target of the (now deleted) controlled operation was, where θ_i is drawn from a normal distribution of mean 0 and variance $\log((1-2p)^{-2})$ for each shot. This has the advantage that it avoids the need to compute exponentially many weights, but with the disadvantage that each shot needs a different circuit. This may or may not be an issue with future quantum compilers.

Another simplification can be made by noting that \mathcal{E}^∞ acting on both qubits (\mathcal{E}_2^∞) produces the same behavior as \mathcal{E}^∞ acting on a single qubit (\mathcal{E}_1^∞) twice. This is a consequence of the fact that \mathcal{E}_2^∞ , \mathcal{E}_U and $|S\rangle$ are all invariant under $|ab\rangle \mapsto |ba\rangle$. This means we can eliminate half of the cost of implementing \mathcal{E}_2^∞ , because acting with \mathcal{E}_1^∞ twice is the same as acting with \mathcal{E}_1^∞ once but with $T_{1/2} \mapsto T_{1,2}/2$. Furthermore, since \mathcal{E}_1^∞ , \mathcal{E}_U and $|S\rangle$ are all also invariant under $|\uparrow\rangle \leftrightarrow |\downarrow\rangle$, we see that

$$\tilde{S}(t) = \langle S | \mathcal{E}_2^\infty(\mathcal{E}_U(|S\rangle\langle S|)) | S \rangle = \langle S | \mathcal{E}_1^0(\mathcal{E}_U(|S\rangle\langle S|)) | S \rangle \quad (14)$$

because any losses in the population of $|\uparrow\downarrow\rangle$ (from $|\uparrow\downarrow\rangle \mapsto |\downarrow\downarrow\rangle$) are exactly offset by the gain in the population of $|\downarrow\uparrow\rangle$ (from $|\uparrow\uparrow\rangle \mapsto |\downarrow\uparrow\rangle$), and the temperature doesn't affect the coherences. This allows us to simply delete the "Temp" part of the circuit in Fig. 1. Note that Eq. 14 does *not* hold if \mathcal{E}_1^0 is replaced by \mathcal{E}_2^0 because losses in the population of $|\uparrow\downarrow\rangle$ are offset by gains in $|\downarrow\uparrow\rangle$ and $|\downarrow\downarrow\rangle$. Putting this all together, we get the circuit shown in Fig. 2.

B. Leveraging Inherent Qubit Noise

An entirely different approach to simulating the thermal relaxation of a system is to try to take advantage of the inherent thermal relaxation of the qubits in the quan-

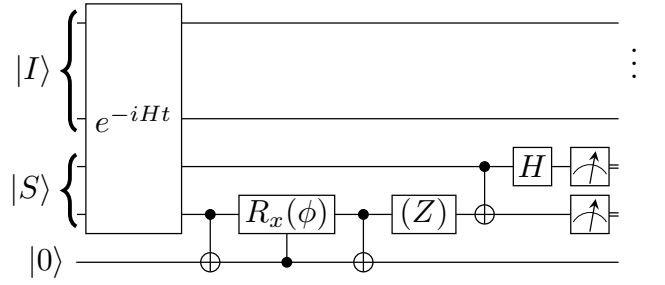


FIG. 2: Circuit to simulate the dynamics of a spin system subject to thermal relaxation using the Kraus method. $\phi = 2 \sin^{-1}(\sqrt{p_x})$ (Z) indicates that the shots are to be split between implementing the circuit including the Z gate and omitting the Z gate. Results are then combined as a weighted average with weights $w_z = p_z$, $w_{\bar{z}} = \bar{p}_z$. The final cX and H gates transform from the Bell basis and map $|S\rangle \mapsto |11\rangle$ for measurement.

tum computer. At the most basic level, the protocol is to simply run the simulation and rely on the qubits' natural decoherence behavior to implement the dissipative channels for free. This approach is appealing since simulating dissipative channels will become increasingly expensive in time and space as system sizes grow. It is also an interesting application of NISQ devices, whose noise often hinders quantum simulation. Here we hope to turn that around and use the noise as an integral part of the simulation. Such a protocol will be most beneficial for NISQ devices when gate errors are sufficiently low and qubit decoherence is the limiting factor in a simulation.

Despite the apparent simplicity, there are a variety of challenges inherent to such an approach. One immediate challenge that arises is that the qubits are an effective zero-temperature system while the spin chemistry systems are effectively infinite temperature. Furthermore, a more practical issue is that during the long time-scales for this protocol systematic errors tend to be amplified. Specifically, the errors from effective $Z \otimes I$ and $I \otimes Z$ terms arising due to qubit frequency miscalibration[53] were particularly problematic in our simulations.

The qubits in IBMQ's machines are always precessing under the action of the Hamiltonian term $\Omega \sigma_z/2$ [54]. I.e. a qubit in state $|\psi\rangle$ at $t = 0$ will evolve to $e^{-i\Omega \sigma_z t/2} |\psi\rangle = R_z(\Omega) |\psi\rangle$ after time t . This precession is corrected for in software, but miscalibrations of Ω will result in imperfect corrections. If the true frequency is Ω but the backend is calibrated to $\omega = \Omega - \Delta\omega$, then after a time t the corrected state will be $R_z(\Delta\omega t) |\psi\rangle$ instead of $|\psi\rangle$.

Because $\Delta\omega t$ tends to be small for t values associated with typical circuits, this error tends to be negligible. However, our circuits run to long enough times where this becomes a significant error. We can mitigate this error by introducing X gates (aka echo pulses) into our circuit, which has the effect of flipping the sign of the phase, so further phase accumulation will cancel instead

of compound[55, 56]. It is easy to verify that using an even number of echo pulses, n , at $(k + 1/2)t/n$, $k \in \{0, 1, \dots, n - 1\}$ corrects this error

$$R_z\left(\frac{\Delta\omega t}{2n}\right) \cdot \prod_{k=1}^n \left[X R_z\left(\frac{\Delta\omega t}{n}\right) \right] \cdot R_z\left(\frac{\Delta\omega t}{2n}\right) = I$$

Additionally, these X gates also have an effect on the decay characteristics of the state. As the qubits are at $T \approx 0$ they are always decaying toward $|0\rangle$. The X gates flip $|0\rangle \leftrightarrow |1\rangle$ so the amplitude damping proceeds “in reverse” while the dephasing is unaffected. One would expect this to be a crude approximation to the infinite temperature amplitude damping where a qubit is decaying toward an equal mixed state of $|0\rangle$ and $|1\rangle$. Indeed as $n \rightarrow \infty$ we recover the exact \mathcal{E}^∞ . Denote the probability of measuring $|S\rangle$ after running the protocol using n (even) echo gates as $S^e(t)$. Then we find

$$\tilde{S}(t) = S^e(t) - \left(\frac{\left(e^{-\frac{t}{T_1}} - 1 \right) \sinh^2\left(\frac{t}{4nT_1}\right)}{\cosh\left(\frac{t}{2nT_1}\right)} \right)^2 \quad (15)$$

and $S^e(t)$ converges to $\tilde{S}(t)$ for all t as n increases. However, increasing n also incurs errors due to imperfect X gates. In this work, we find using $n = 4$ gives good results and the corresponding circuit is shown in Fig. 3.

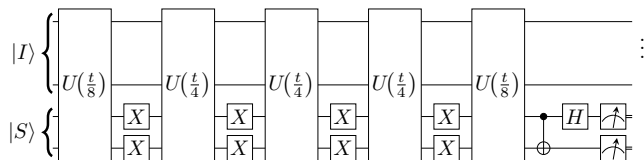


FIG. 3: Circuit to simulate the dynamics of a spin system subject to thermal relaxation using the Inherent method where $U(t) = e^{-iHt}$. The final cX and H gates transform from the Bell basis and map $|S\rangle \mapsto |11\rangle$ for measurement.

Another potential issue is that the T_1 and T_2 of the qubits may be significantly longer than typical simulation times. Typically the timescales for decoherence in superconducting qubits are 10s of microseconds[54] and potentially much longer for other technology, like trapped ions[57].

This issue can be overcome by slowing the execution of the circuit. This can potentially be done by, for example, pulse stretching[58], using large numbers of small Trotter steps and/or adding wait cycles into the circuit. Pulse stretching is especially appealing because it is continuously applying \mathcal{E}_U while \mathcal{E}^0 is naturally occurring, overcoming the issue associated with the fact that $[\mathcal{E}_U, \mathcal{E}^0] \neq 0$. It also uses fewer gates than applying a large number of small trotter steps. Adding in wait cycles between trotter steps is the easiest to implement but also incurs the largest error due to $[\mathcal{E}_U, \mathcal{E}^0] \neq 0$.

Additionally, the ratio T_1/T_2 may be quite different between the radical pair and the qubits. One can always use the Kraus method above to implement dephasing to lower T_2 as far as desired. We show another general approach in the following subsection that can be used to fix the decoherence parameter mismatch between qubits and radical pairs.

C. Correction Circuits

In principle, the time evolution and decoherence can be run separately and the results combined in a classical post-processing step to recover the full dynamics. We do this as follows:

Step 1) Implement the time evolution with no decoherence, i.e. use the circuit in Fig. 2 without the decoherence part. Let the measured populations of $\{|S\rangle, |T_0\rangle, |T_\pm\rangle\}$ for this step be $\{S, T_0, T_\pm\}$ respectively.

Step 2) In parallel, apply decoherence to the singlet state with no coherent time evolution, i.e. use circuit in Fig. 2 with $t = 0$ or Fig. 3 with $U(t)$ replaced by identity gates. Let the measured populations of $\{|S\rangle, |T_0\rangle, |T_\pm\rangle\}$ for this step be $\{S', T'_0, T'_\pm\}$ respectively.

Step 3) Combine the results from steps 1 and 2 to recover the thermally relaxed dynamics, \tilde{S}

$$\tilde{S} = SS' + T_0T'_0 + T_+T'_+ + T_-T'_- \quad (16)$$

Because of the symmetry in \mathcal{E}^∞ , the probability of $|S\rangle \mapsto |T\rangle$, where $|T\rangle$ is any triplet state, is equal to the probability $|T\rangle \mapsto |S\rangle$. In this way we can view $\{S, T_0, T_\pm\}$ as the undamped populations and $\{S', T'_0, T'_\pm\}$ as the probability of those states transitioning to $|S\rangle$.

This method can be used to add decoherence to a simulation implemented without decoherence. Additionally, this method can be used to “undo” any decoherence occurring during a simulation, which is often unavoidable on NISQ devices. Given simulation results subject to T_1 and T_2 decay i.e. $\{\tilde{S}, \tilde{T}_0, \tilde{T}_\pm\}$ and $\{S', T'_0, T'_\pm\}$, this provides a procedure to recover the undamped dynamics. This can be done by using Eq. 16 together with

$$\begin{aligned} \tilde{T}_0 &= T_0S' + ST'_0 + T_+T'_+ + T_-T'_- \\ \tilde{T}_\pm &= T_+ + T'_+ - 4T_+T'_+ \end{aligned} \quad (17)$$

to solve for the undamped populations $\{S, T_0, T_\pm\}$.

Furthermore, the ability of correction circuits to both apply and “undo” decoherence allows for more flexible decoherence protocols. In particular when using the inherent method, if the qubits have a T_1/T_2 value which is different from that of the radical pairs, the decoherence dynamics of the qubits will not mimic that of the system. In this situation, we can apply the correction circuit procedure twice to fix these issues and recover the desired

decay dynamics of the radical pair system. The idea is to first use the correction circuit method to “undo” the decoherence from the qubits and then use the method a second time in conjunction with the Kraus method to apply the desired decoherence.

To do this, we perform the time evolution with decoherence using the inherent method yielding $\{\tilde{S}, \tilde{T}_0, \tilde{T}_\pm\}$. We also perform the decoherence using the inherent method without time evolution, giving us $\{S', T'_0, T'_\pm\}$. Next, we decohere the singlet state using the Kraus method (circuit in Fig. 2 without the time evolution), inputting the desired T_1 and T_2 parameters, giving $\{S'', T''_0, T''_\pm\}$. We then use $\{\tilde{S}, \tilde{T}_0, \tilde{T}_\pm\}$ and $\{S', T'_0, T'_\pm\}$ to recover $\{S, T_0, T_\pm\}$ via Eqs. 16, 17 and then apply Eq. 16 with these values and $\{S'', T''_0, T''_\pm\}$ to produce the correct $\tilde{S}(t)$ with the radical pair and qubits having arbitrary T_1 and T_2 values. In certain situation, e.g. $T_1 \rightarrow \infty$ as outlined in the next section, this protocol may simplify.

IV. APPLICATIONS

In this section we benchmark our methods by using them to simulate two different radical pair systems that have been previously studied in spin chemistry experiments. The first pair consists of a perdeuterated para-terphenyl radical anion (PTP) and a perdeuterated diphenyl sulphide radical cation (DPS) and the second pair consists of a 2,2,6,6-tetramethylpiperidine radical cation (TMP) and PTP. The chemical structures of these species are shown in Fig. 4.

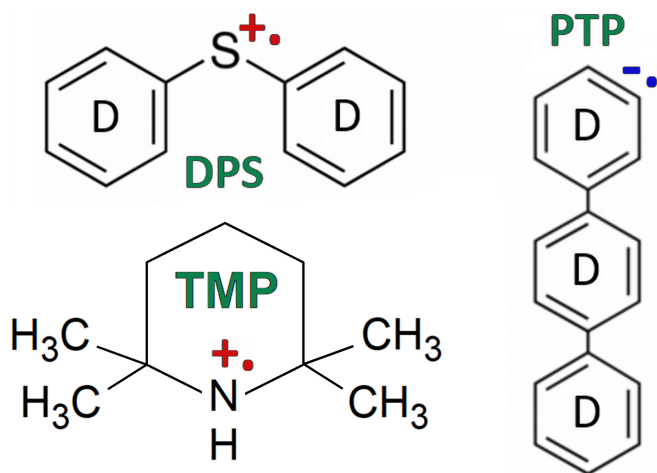


FIG. 4: Chemical structures of radical ions DPS, TMP and PTP which are used in the remainder of the paper.

A. Quantum beats in diphenyl sulfide-d₁₀⁺ (DPS) / para-terphenyl-d₁₀⁻ (PTP)

We begin with an application to a very simple system, the radical pair perdeuterated diphenyl sulfide⁺ (DPS) and perdeuterated para-terphenyl⁻ (PTP) in a dilute alkane solution. In this system, hyperfine couplings observed in the experiment are largely negligible due to the much smaller magnetic moment of deuteron, and due to fast ion-molecule electron exchange among the diphenyl sulfide molecules in solution[43]. However, while largely negligible, the large number of small hyperfine couplings can be approximated semi-classically by treating the effects of these couplings as a Gaussian dephasing term[59]. In this case, the expression Eq. 13 for $\tilde{S}(t)$ becomes[43]:

$$\tilde{S}(t) = \frac{1}{4} \left(1 + e^{-t/T_1} + e^{-t/T_2 - \sigma^2 t^2} (4S(t) - 2) \right) \quad (18)$$

Where[59] $\sigma = \sqrt{\frac{1}{3} \sum_n a_n^2 I_n(I_n + 1)}$ is the second moment of the Gaussian distribution of the hyperfine components. This is interesting to note, because superconducting qubits are also potentially subject to such broadband dephasing processes from things like flux noise, charge noise and critical-current noise[60]. Indeed we did observe Gaussian type dephasing noise in some of our runs, but until these noise sources are more predictable and well documented, it will be difficult to leverage this noise as a resource.

If we neglect the HFC in PTP, we can directly simulate the Hamiltonian time evolution on currently available devices - due to the simple form the Hamiltonian takes:

$$H = \mu_B \mathbf{B} \cdot (g_1 \mathbf{S}_1 + g_2 \mathbf{S}_2) \propto \alpha S_1^z + \beta S_2^z. \quad (19)$$

where $g_1 = 2.0028$, $g_2 = 2.0082$, $\mathbf{B} = B\hat{z}$ and $B = 17\text{mT}$ for low-field and 960mT for high-field[43]. Note that this simple Hamiltonian gives

$$U(t) = e^{-iHt} = R_z(\omega_1 t) \otimes R_z(\omega_2 t)$$

where ω_i is proportional to g_i . In this case, with no hyperfine couplings present in both radicals, singlet-triplet ($|S\rangle \leftrightarrow |T_0\rangle$) oscillations in external magnetic field result from the difference in Larmor precession rates of the two electron spins caused by difference in their g-factors with no transitions to $|T_\pm\rangle$. The singlet state population in this case is described by the expression[24]

$$S_B(t) = \cos^2 \left(\frac{\omega_1 - \omega_2}{2} t \right) \quad (20)$$

Since the Hamiltonian is composed of only S^z operators, it's easy to see that $[\mathcal{E}_U, \mathcal{E}^0] = 0$. This allows us to do all of the time evolution in one step and then the decoherence in the next. For this system, we employ the

inherent method (Sec. III B). For this simple case, the time evolution is accomplished with R_z gates and the decoherence step is just the echo pulses with pauses in between. We implement the pauses in IBMQ by using identity gates, which act as wait cycles. We choose the number of identity gates to use as

$$N = \frac{t T_{qu}}{T_{rp} t_{id}} \quad (21)$$

where t is the simulated time, T_{qu} is the average of T_1 and T_2 over both qubits, T_{rp} is the decay time of the radical pairs and t_{id} is the duration of the identity gate. T_{qu} and t_{id} are provided by the backend in Qiskit. The circuit implementing this protocol is shown in Fig. 5.

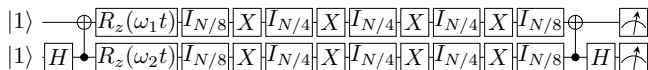


FIG. 5: Circuit to simulate the dynamics and thermal relaxation of the DPS/PTP radical pair. I is the identity gate, N is given by 21 and $\omega_i \propto g_i$. $\tilde{S}(t)$ is given as the probability of measuring $|11\rangle$. This circuit uses four echo pulses (XX gates) to mitigate errors from frequency miscalibration and to approximate the infinite temperature dynamics. The deviation from the true infinite temperature dynamics is given in Eq. 15. Over the time range simulated, the maximum deviation between the theoretical $\tilde{S}(t)$ and the ideal result of this circuit is less than 3×10^{-5} .

As a proof of concept of the Inherent method (Sec. III B), we begin by simulating the circuit shown in Fig. 5, with thermal noise added to the qubits using Qiskit AER’s “thermal relaxation error” noise model. Qiskit takes as input the qubits temperature (0), time, T_1 and T_2 and then simulates the circuit assuming the qubits thermally relax following amplitude damping and dephasing. Additionally, we generate the semi-classical broadband dephasing noise (σ from Eq. 18) by modifying Qiskit AER’s “thermal relaxation error” module to assess the effect of neglecting the HFC in PTP. Note that one can easily implement this semi-classical dephasing on a quantum computer using the Kraus method outlined in Sec. III A at essentially no computational cost. We run both circuits at 5,000 shots, which matches our runs on the actual quantum computers.

These results are shown in Fig. 6a and are in excellent agreement with both theory and experiment. We find that for PTP, the semi-classical hyperfine coupling approximation gives a correction much smaller than the other sources of uncertainty (e.g. experimental uncertainty in T_1/T_2 values[43]) and so we will neglect it moving forward.

Having confirmed the validity of neglecting the HFC in PTP, we proceed to run the circuit shown in Fig. 5 on IBMQ’s Toronto quantum computer for both high- and low-field. These results are shown in Fig. 6b and show

excellent agreement with the theory. We do note that our high-field run appears to have been subjected to some broadband dephasing noise, which becomes apparent at long times, in addition to the expected dephasing and amplitude damping.

The data from Fig. 6b is then combined to calculate $\tilde{M}(t)$ as per Eq. 2, using $\theta = 0.425$ [43]. The result is shown in Fig. 6c alongside the experimental results[43] as well as our theoretical calculation. The simulation data are in excellent agreement with both the experimental and theory data, aside from the minor effects of broadband dephasing at long times.

B. Quantum beats in 2,2,6,6-tetramethylpiperidine⁺/para-terphenyl-d₁₄⁻

Now looking at another system, we consider the radical pair 2,2,6,6-tetramethylpiperidine⁺ (TMP) and para-terphenyl-d₁₄⁻ (PTP). As before, this radical pair can be formed by the passage of a burst of radiation through the solution of the two compounds, resulting in ionization of solvent molecules and subsequent capture of electrons by PTP molecules and holes by TMP molecules.

TMP is a radical cation, and its unpaired electron spin is localized on the nitrogen atom. There are two magnetic nuclei interacting with the electron spin, nitrogen with a nuclear moment of 1, and amine hydrogen with a nuclear moment of $\frac{1}{2}$.

In the PTP radical anion the unpaired electron spin density is delocalized, and hyperfine couplings are very small due to small magnetic moments of the deuterium nuclei and are neglected in this treatment, as justified in Sec. IV A. However, the HFC in TMP cannot be neglected because the electron density is localized and the couplings are much stronger.

The Hamiltonian describing this system is

$$H = \mu_B \mathbf{B} \cdot (g_1 \mathbf{S}_1 + g_2 \mathbf{S}_2) + a_H \mathbf{I}_H \cdot \mathbf{S}_1 + a_N \mathbf{I}_N \cdot \mathbf{S}_1 \quad (22)$$

Here \mathbf{S}_1 and \mathbf{S}_2 refer to the electron spins in TMP and PTP respectively, \mathbf{I}_i refers to the nuclear spin of species i and \mathbf{B} is the magnetic field. This is similar to the DPS/PTP Hamiltonian (Eq. 19), with the addition of hyperfine couplings to the nitrogen and hydrogen nuclei on the TMP (last two terms in the Hamiltonian). The hydrogen and nitrogen HFC constants determined experimentally are $a_H = -1.87\text{mT}$, and $a_N = 1.8\text{mT}$ [28].

One large difference between the TMP and DPS radical pair with PTP is that the T_1 decay time is dependent on the magnetic field for TMP/PTP. In particular, we have $T_1 = T_2$ for the low-field but $T_1 \gg T_2$ for the high field. Therefore, to use the inherent method for high field, we will need to invoke a correction circuit as described in section III C. This will be described in more detail below.

Simulating the coherent time evolution under this Hamiltonian is no longer trivial like for DPS/PTP. As of this writing, simulating this system out to times of interest is beyond the capabilities of current quantum com-

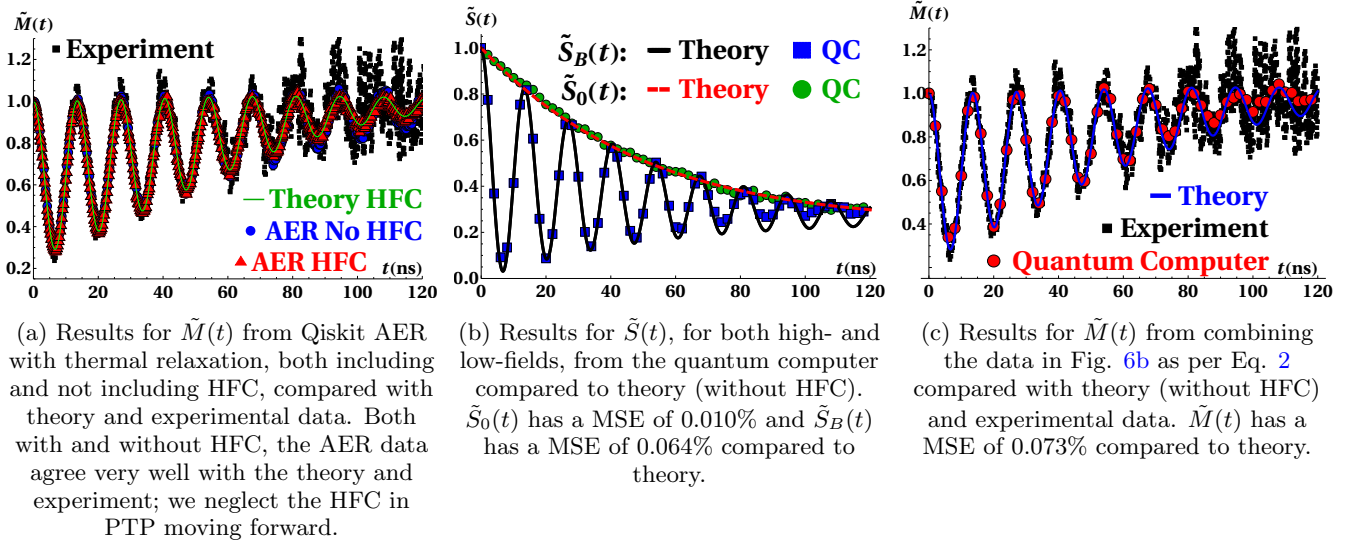


FIG. 6: Data for the TR MFE ($\tilde{M}(t)$) and $\tilde{S}(t)$ at high- and low-fields from running the Inherent method for the DPS/PTP radical pair (circuit in Fig. 5) vs. theoretical calculations and experimental data. Runs were conducted by simulating our circuit in Qiskit AER with thermal noise as well as on IBM’s Toronto quantum computer, both using 5,000 shots. For runs including the HFC of PTP we take $T_1 = T_2 = 60\text{ns}$ and take $T_1 = T_2 = 50\text{ns}$ for runs without HFC. $\tilde{M}(t)$ is constructed from $\tilde{S}(t)$ as per Eq. 2 with $\theta = 0.425$ [43, 61]

puters. Because using the quantum computer to simulate $S(t)$ directly is not yet feasible, we demonstrate our protocols by classically precomputing $S(t)$, as described in II A, and encoding it onto a pair of qubits.

Fig. 7a shows the classical precomputation of $S(t)$, as computed by Eq. 5 for $B = 0$ and $B = 0.1\text{T}$, the values used in the experiment.

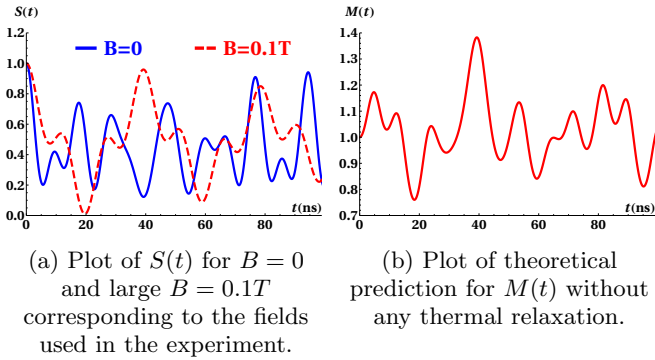


FIG. 7: Theoretical calculation of the quantities of interest without any thermal relaxation.

These are then combined as per Eq. 2 to yield $M(t)$, shown in Fig. 7b. Encoding $S(t)$ onto the qubits is simple and is accomplished with the circuit shown in Fig. 8.

With $S(t)$ encoded on the qubits, we may directly apply the Kraus method. Note that although this encoding of $S(t)$ onto the qubits does not reproduce the correct electronic state in full (since this encoding does not induce transitions to $|T_{\pm}\rangle$), the resulting $\tilde{S}(t)$ is the same.

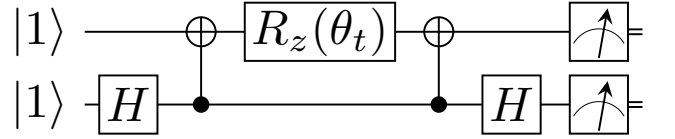


FIG. 8: Raw circuit returning $S(t)$, the probability of the TMP/PTP radical pair being in a singlet state at time t , as the probability of measuring $|11\rangle$. Note that $S(t)$ is explicitly encoded in $\theta_t = 2 \cos^{-1}(\sqrt{S(t)})$.

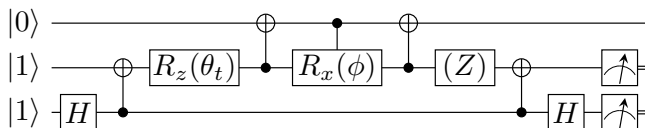
For this situation, we use the circuits in Fig. 9 to implement the Kraus method for low- and high-field dynamics.

The results of running these circuits on an actual quantum computer (IBMQ Toronto at 5,000 shots) are shown in Fig. 12. In general, they agree well with the theory and experimental data across the entire range of simulated time.

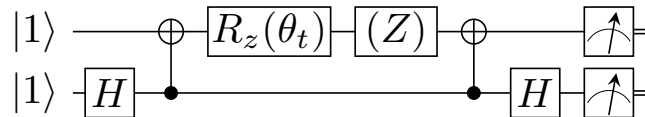
Because $T_1 \gg T_2$ for the high-field case, an implementation of the Inherent method must use a correction circuit (shown in Fig. 10) as outlined in section III C.

However, since our encoding of $S(t)$ onto the qubits doesn’t induce transitions to $|T_{\pm}\rangle$, this greatly simplifies the use of the correction circuit. This happens because any population in $|T_{\pm}\rangle$ can only come from T_1 decay. Since we wish to simulate $T_1 \rightarrow \infty$, we can simply take our $T_1 = T_2$ result and add the population of $|T_{\pm}\rangle$ from the correction circuit, in effect “repopulating” the singlet state with any probability that leaked into $|T_{-}\rangle$ from the T_1 decay.

Denote the probability of measuring the singlet state



(a) Circuit for $B = 0$. Both amplitude damping and dephasing must be considered. $\theta_t = 2 \cos^{-1}(\sqrt{S_0(t)})$, $\phi = 2 \cos^{-1}(e^{-t/(2\tau)})$ and $w_z = \frac{1}{2}(1 - e^{-t/(2\tau)})$



(b) Circuit for large B . Only dephasing needs to be considered. $\theta_t = 2 \cos^{-1}(\sqrt{S_B(t)})$ and $w_z = \frac{1}{2}(1 - e^{-t/T_2})$

FIG. 9: Circuits to simulate the thermal relaxation of our system. The singlet state corresponds to measuring $|11\rangle$. (Z) indicates that the shots are to be split between implementing the circuit including the Z gate and omitting the Z gate. Results are then combined as $S = w_z P_{11}^Z + (1 - w_z) P_{11}^{\text{no } Z}$

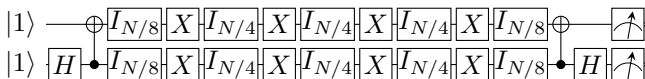


FIG. 10: Correction circuit (Sec. III C) for use with Inherent method (Sec. III B). I_n means apply n identity gates.

(i.e. $|11\rangle$) from the circuit shown in Figs. 11 as $P(S)$ and the probability of measuring $|T_-\rangle$ (i.e. $2|00\rangle$) from the correction circuit shown in Fig. 10 as $P(T)$. Then we have $\tilde{S}(t) = P(S) + P(T)$. Both $P(S)$ and $\tilde{S}(t)$ are shown in Fig. 12b. While this is a nice simplification for our case, it will not work when doing true Hamiltonian simulation and the more involved method described in section III C must be used.

The results from running the circuits which are shown in Figs. 10 (Simulation) and 11 (Correction) are shown in Figs. 12a and 12b. The final results for the TR-MFE obtained by classically combining the low- and high-field results are shown in Fig. 12c. For this system we used a combination of all three methods, and find excellent agreement with theory. The Kraus method gives a MSE of 0.015% and the Inherent method + correction circuit gives a MSE of 0.0059% compared to theory. Our results are less noisy than the experimental data which, even after removing the anomalous data from $t = 0$ to $t = 12$, have a MSE of 0.109%.

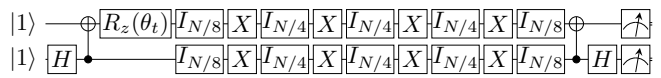


FIG. 11: Circuit to implement the dynamics and thermal relaxation using the inherent method. I_n means apply n identity gates.

V. CONCLUSION

We have shown that thermal relaxation may be added to a spin chemistry simulation effectively on a quantum computer, with minimal added resources. This can be done by explicitly simulating the thermal relaxation Kraus operators (Sec. III A), by leveraging the inherent thermal relaxation of the qubits themselves (Sec. III B), or by separately running the simulation without thermal relaxation and a correction circuit undergoing relaxation (using either previous method) and combining the results in a classical post-processing step (Sec. III C).

The Kraus method provides the most control over the thermal relaxation, providing full control over the relaxation parameters such as temperature, T_1 and T_2 . However, this method is only suitable when the simulation can be performed in a time much shorter than the qubits' natural decoherence time. Otherwise, the qubits' natural decoherence will interfere with the artificial Kraus decoherence, leading to inaccurate results. This issue can be mitigated by using the correction circuit method outlined in Sec. III C. Furthermore, implementing the Kraus method requires ancilla qubits and controlled rotations which makes it unlikely to generalize well to larger systems on NISQ devices. An exception is when only dephasing is required which may be done at any scale, practically for free, by using R_z gates with their angles drawn from a normal distribution each shot. Furthermore, when the Kraus map doesn't commute with the system's unitary time evolution (e.g. $T \neq \infty$), the map must be Trotterized and implemented each time step, further adding to the cost.

Alternatively, leveraging the inherent thermal relaxation of the qubits suffers none of these problems - remaining virtually free to implement for any system size and utilizing the qubits natural decoherence as a resource. However, it is much more restrictive in its applicability since the relaxation parameters of the qubits is fixed. We have shown some examples of how to get around these constraints by invoking a correction circuit to map the natural qubit relaxation dynamics onto the relaxation dynamics of a system of interest.

Furthermore, we show how this correction circuit can be used to invert the relaxation of a simulation to recover the un-relaxed dynamics as well as to add relaxation to the results of an un-relaxed simulation. More study is needed to determine how widely applicable such methods are to simulations outside of those described by Hamiltonians of the form given in Eq. 3.

We demonstrate the effectiveness of these techniques

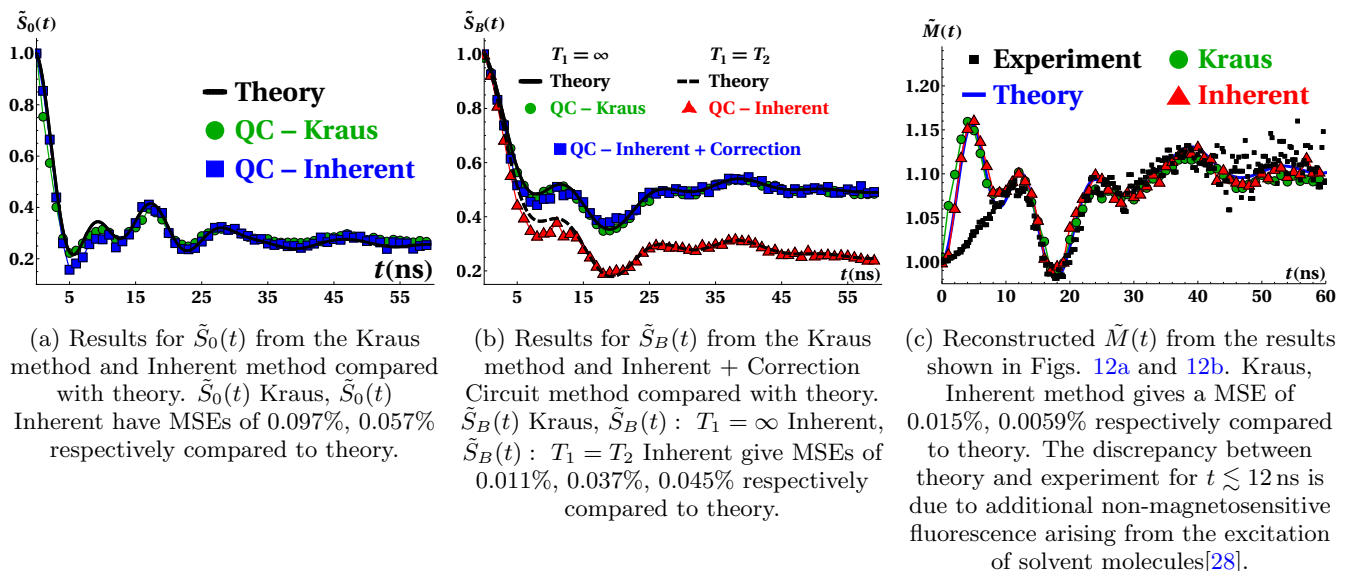


FIG. 12: Data for the TR MFE ($\tilde{M}(t)$) and $\tilde{S}(t)$ at high- and low-fields from running both the Kraus and Inherent + Correction Circuit methods for the TMP/PTP radical pair (circuits in Figs. 9, 11, 10) vs. theoretical calculations and experimental data. Runs for the Kraus method were conducted on IBM’s Almaden quantum computer, the other circuits were conducted on IBM’s Toronto quantum computer, all runs used 5,000 shots. $\tilde{M}(t)$ is constructed from $\tilde{S}(t)$ as per Eq. 2 with $\theta = 0.108$. The results are highly accurate for both methods, which is not terribly surprising given the simplicity of these circuits due to bypassing the Hamiltonian simulation step.

on two simple, real-world systems of interest in spin chemistry. Due to the simplicity of the DPS/PTP radical pair system, we are able to implement the full Hamiltonian simulation. Using the Inherent method, we were able to reproduce the theoretical result for the TR MFE with a mean squared error of 0.073% (Fig. 6), despite the presence of broadband dephasing seen at longer times. This shows that such methods are an effective tool to model real world systems undergoing thermal relaxation that is usable on currently available quantum devices. Furthermore, these results are significantly less noisy than the experimental data (MSE 0.97%), which suffers from a noise problem outlined in Appendix B.

We also demonstrate the effectiveness of these techniques for a more complicated system (the TMP/PTP radical pair) having two hyperfine coupling terms and a B -field dependent T_1 relaxation rate. Unfortunately, currently available quantum computers aren’t sufficiently robust enough to implement Hamiltonian simulation of this system - largely due to CNOT error rates. As quantum computers continue to improve gate fidelity, we hope in the near future this will be possible. In order to work around this, we classically precompute $S(t)$, encode this onto a pair of qubits and use our protocols to recover $\tilde{S}(t)$. This classical precomputation step is exponentially hard in the size of the nuclear degrees of freedom, making it desirable to develop optimal methods for Hamiltonian time evolution on a quantum computer.

The results for TMP/PTP using both the Kraus and inherent + correction circuit method are shown in Fig.

12. We find excellent agreement with theory, with both of our datasets again being less noisy than the experimental data. When directly simulating time evolution becomes reliable on NISQ devices, the encouraging results here suggest our methods could provide fast, easy and cheap ways to do primary investigations into spin chemistry problems to direct or supplement experiments. Because these methods do not suffer from the experimental noise problem outlined in Appendix B, they may also provide a way to probe experimentally inaccessible regimes.

Further research is needed to explore the applicability of the three methods presented here to Hamiltonians other than those of the form in Eq. 3. It is likely that these methods will be applicable to many systems relaxing in an effectively infinite temperature environment.

VI. ACKNOWLEDGMENTS

We thank Dan Rugar, John Mamin, Andrew Eddins and Andrew Cross of IBM for their helpful discussions and insight that lead to the use of echo pulses in our protocol. We thank Dr. V.A. Bagryansky (V.V. Voevodsky Institute of Chemical Kinetics and Combustion, Novosibirsk, Russia) for allowing use of his experimental data on quantum beats. This work was supported by the U.S. Department of Energy, Office of Science, Basic Energy Sciences, Division of Materials Sciences and Engineering under Grant No. de-sc0019469. B. R. was also supported by the National Science Foundation

under Award DMR-1747426 (QISE-NET). M. V. is supported by the IBM Global University Program. We acknowledge the use of IBM Q for this work. The views expressed are those of the authors and do not reflect the official policy or position of IBM or the IBM Q team.

Appendix A: Commutation of Time Evolution and Decoherence Channels

It is fairly simple to show that the generalized amplitude damping, \mathcal{E}_x , and dephasing, \mathcal{E}_z , channels commute. Note that sufficient (but not necessary) condition for two quantum channels to commute is that all of the Kraus operators from the two channels satisfy $K_i^1 K_j^2 = e^{i\phi} K_j^2 K_i^1$. This follows directly from Eq. 6 and 9 because all of the phases simply cancel, $K \rho K^\dagger = (e^{i\phi} K) \rho (e^{i\phi} K)^\dagger$.

It is easy to see then that \mathcal{E}_x and \mathcal{E}_z commute because $K_i^x K_j^z = \pm K_j^z K_i^x$ which follows directly from anti-commutation relations of the Paulis and the form of the Kraus operators in Eqs. 7 and 8. Let $\mathcal{E}(\cdot) \equiv \mathcal{E}_x(\mathcal{E}_z(\cdot))$.

It is less obvious that coherent time evolution and \mathcal{E} commute, largely because it is untrue. However, we show that at laboratory temperatures the time evolution of *only* the electronic DOFs commutes with \mathcal{E} . Denote \mathcal{E} operating at infinite temperature to be \mathcal{E}^∞ .

We argue as follows, by tracing out the nuclear subsystem we are formally treating it as a finite bath interacting with the electronic subsystem. The interaction can be read off of Eq. 3 and is given by

$$\sum_{i,j} a_{ij} \mathbf{I}_{ij} \cdot \mathbf{S}_i = \sum_{i,j} \frac{a_{ij}}{2} (I_{ij}^+ S_i^- + I_{ij}^- S_i^+ + 2I_{ij}^z S_i^z). \quad (\text{A1})$$

The two terms involving S^\pm can be thought of as performing amplitude damping. Because the initial nuclear state is the maximally mixed state, i.e. the infinite temperature state, this interaction applies infinite temperature amplitude damping. The term involving S^z performs the phase damping channel. As such, the interaction between the electronic and nuclear subsystems performs \mathcal{E}^∞ on the electronic subsystem. Since \mathcal{E}^∞ trivially commutes with itself, it is not surprising that the coherent time evolution and decoherence channel commute as well. We now make the argument more precise, although a rigorous proof is beyond the scope of this work.

The action of coherent time evolution, from an initial time $t = 0$ to t , on the electronic subsystem only is itself represented by a quantum channel, \mathcal{E}_U . The Kraus operators for \mathcal{E}_U are given by

$$K_{ij}^U = \sqrt{P(|\mathbf{I}_i\rangle)} |\mathbf{I}_i\rangle e^{-iHt} |\mathbf{I}_j\rangle \quad (\text{A2})$$

such that

$$\rho_U = \mathcal{E}_U(\rho(0)) = \sum_i |\mathbf{I}_i\rangle e^{-iHt} \rho(0) e^{iHt} |\mathbf{I}_i\rangle \quad (\text{A3})$$

where the sum traces out the nuclear DOF and

$$\langle \mathbf{I}_i | \hat{A} | \mathbf{I}_i \rangle = \sum_{j,k} \langle \mathbf{I}_i, e_j | \hat{A} | \mathbf{I}_i, e_k \rangle |e_k\rangle \langle e_j|. \quad (\text{A4})$$

Here $|\mathbf{I}_i\rangle (|e_i\rangle)$ is the i^{th} basis state for the nuclear (electronic) subsystem, $P(|\mathbf{I}_i\rangle)$ is the probability of being in that nuclear state at $t = 0$ and ρ_U is the state of the electronic subsystem at time t . For our case the initial nuclear state is the maximally mixed state, $P(|\mathbf{I}_i\rangle) = P = 1/N_{\mathbf{I}}$. From here, a few observations may be made. For simplicity we take $\rho(0) = |S\rangle \langle S|$ moving forward, although the argument holds for any initial state of the form $\rho(0) = e^{-i\alpha H} |S\rangle \langle S| e^{i\alpha H}$.

Transitions from the singlet state $|S\rangle$ to either triplet state with $m_s \neq 0$ ($|T_+\rangle = |\uparrow\uparrow\rangle$, $|T_-\rangle = |\downarrow\downarrow\rangle$) occur from the terms containing an S_i^\pm in Eq. A1. These terms come with a corresponding, distinct transition in the nuclear state from I_{ij}^\pm . Furthermore, due to symmetry in the Hamiltonian, and therefore in Eq. A1, the probability of transition to $|T_+\rangle$ is equal to $|T_-\rangle$. Due to spin conservation, a nuclear state corresponding the electronic state being in either $|T_\pm\rangle$, cannot correspond to any other electronic state. From Eqs. A3 and A4 then, we see ρ_U has a term of $a(|T_+\rangle \langle T_+| + |T_-\rangle \langle T_-|)$ and no other terms involving $|T_\pm\rangle$.

Likewise, transitions from $|S\rangle$ to $|T_0\rangle = \frac{1}{\sqrt{2}}(|\uparrow\downarrow\rangle + |\downarrow\uparrow\rangle)$ mediated by nuclear interactions will contribute a term of $b|T_0\rangle \langle T_0|$. Finally, evolution that leaves the nuclear state unchanged, i.e. evolution mediated by \mathbf{B} , coherently rotates between $|S\rangle$ and $|T_0\rangle$. This contributes a term to ρ_U of the form $c(R_z(\phi) \otimes R_z(\varphi)) |S\rangle \langle S| (R_z(-\phi) \otimes R_z(-\varphi))$. Explicitly writing this out gives

$$\rho_U = \begin{pmatrix} & |\uparrow\uparrow\rangle & |\downarrow\downarrow\rangle & |\uparrow\downarrow\rangle & |\downarrow\uparrow\rangle \\ |\uparrow\uparrow\rangle & a & 0 & 0 & 0 \\ |\downarrow\downarrow\rangle & 0 & b+c & b-ce^{-i\theta} & 0 \\ |\uparrow\downarrow\rangle & 0 & b-ce^{i\theta} & b+c & 0 \\ |\downarrow\uparrow\rangle & 0 & 0 & 0 & a \end{pmatrix} \quad (\text{A5})$$

where normalization implies $a = \frac{1}{2} - b - c$ and we've defined $\theta = \phi - \varphi$. It is much more straightforward to show that $\rho_D = \mathcal{E}^\infty(\rho(0)) =$

$$\frac{1}{4} \begin{pmatrix} 1 - \bar{p}_x^2 & 0 & 0 & 0 \\ 0 & \bar{p}_x^2 + 1 & -2\bar{p}_x \mathcal{P}_z^2 & 0 \\ 0 & -2\bar{p}_x \mathcal{P}_z^{*2} & \bar{p}_x^2 + 1 & 0 \\ 0 & 0 & 0 & 1 - \bar{p}_x^2 \end{pmatrix} \quad (\text{A6})$$

where $\mathcal{P}_z = 1 - 2p_z$. If we then modify this slightly by adding an $R_z(\phi/2)$ gate to act on one of the qubits before acting with \mathcal{E}^∞ , we get the same result as in Eq. A6 but with $\mathcal{P}_z \mapsto e^{i\phi} \mathcal{P}_z$. A lone $R_z(\phi/2)$ itself defines a quantum channel, $\mathcal{E}^z(\rho) = R_z(\phi/2) \rho R_z^\dagger(\phi/2)$.

It is now explicitly obvious that this new $\mathcal{E}^\infty \circ \mathcal{E}^z$ map implements the same transformation as \mathcal{E}_U , i.e. $\mathcal{E}_U(\rho(0)) = \mathcal{E}^\infty(\mathcal{E}^z(\rho(0)))$. By the same logic that showed

\mathcal{E}_x and \mathcal{E}_z commute, it is easy to see that \mathcal{E}^z and \mathcal{E} commute. Furthermore, since \mathcal{E} commutes with itself, we conclude that \mathcal{E}^∞ and \mathcal{E}_U must themselves commute. Note that for $T \neq \infty$ or for a different Hamiltonian, e.g. one that contains direct interactions between the two species, the above no longer holds.

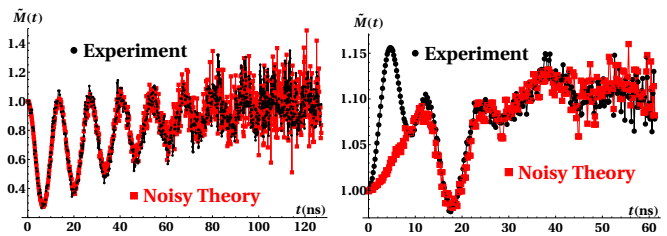
Appendix B: Noise in Experimental Data

The TR MFE is calculated as per Eq. 2 in order to cancel $F(t)$ from 1. This is sound as $F(t)$ has no B dependence, however $F(t)$ is a rapidly decaying function representing lifetime distribution of the radical pairs. So relative noise in the experiment grows for long times as $F(t)$ damps the signal while the noise stays approximately constant.

More technically, $F(t)$ for radical pairs is well approximated by[24, 62]

$$F(t) \approx Ae^{-t/t_1} + B \left(1 + \frac{t}{t_2}\right)^{-\alpha} \quad (\text{B1})$$

with best fit parameters $A = 3.12 \times 10^6$, $B = 2.21 \times 10^5$, $t_1 = 3.47\text{ns}$, $t_2 = 123\text{ns}$, $\alpha = 6.11$ for TMP/PTP as determined by non-linear regression. And $A = 1.317 \times 10^6$, $B = 6.658 \times 10^5$, $t_1 = 2.1432\text{ns}$, $t_2 = 5.1549\text{ns}$, $\alpha = 1.223$ for DPS/PTP[62, 63].



(a) DPS/PTP with $\mu = 0$ and $\sigma = 700$. (b) TMP/PTP with $\mu = 0$ and $\sigma = 75$.

FIG. 13: Comparisons of noise seen in experimental data vs. noise from assuming Gaussian background noise on the detectors in an otherwise ideal experiment. $\bar{M}(t)$ is constructed by adding independent Gaussian noise to $\tilde{S}_0(t)$ and $\tilde{S}_B(t)$ at each time point. We see that such a simple model reproduces the data well and explains the main effect behind increasing noise in the TR MFE vs. time.

We assumed that the PMT detector is a primary source of noise in the experimental data. We approximated the PMT noise with white noise following a normal distribution and applied it to both the high-field and low-field theoretical recombination fluorescence functions, $I(t)$ (Eq. 1) constructed from Eqs B1, 13. We then reconstruct the TR MFE (Eq. 2) using these noisy data. The result is shown in Fig. 13b.

We find a normal distribution of $\mu = 0$ and $\sigma = 75$ reproduces the noise behavior from the experiment very well. Such errors are an inherent challenge to producing good experimental data out to long times. In this regard, performing a quantum simulation opens the potential to investigate the behavior of such systems in finer detail and to longer times than is possible in experiments - once Hamiltonian simulation becomes feasible on these machines.

-
- [1] H. Matsuoka and O. Schieman, in *Electron Spin Resonance (ESR) Based Quantum Computing* (Springer New York, 2016) pp. 51–77.
- [2] M. Atzori and R. Sessoli, *Journal of the American Chemical Society* **141**, 11339 (2019).
- [3] M. D. E. Forbes, *ChemPhotoChem* **3**, 971 (2019).
- [4] P. J. Hore, K. L. Ivanov, and M. R. Wasielewski, *The Journal of Chemical Physics* **152**, 120401 (2020).
- [5] J. N. Nelson, M. D. Krzyaniak, N. E. Horwitz, B. K. Rugg, B. T. Phelan, and M. R. Wasielewski, *The Journal of Physical Chemistry A* **121**, 2241 (2017).
- [6] Y. Wu, J. Zhou, J. N. Nelson, R. M. Young, M. D. Krzyaniak, and M. R. Wasielewski, *Journal of the American Chemical Society* **140**, 13011 (2018).
- [7] J. N. Nelson, J. Zhang, J. Zhou, B. K. Rugg, M. D. Krzyaniak, and M. R. Wasielewski, *The Journal of Chemical Physics* **152**, 014503 (2020).
- [8] K. M. Salikhov, *Uspekhi Fizicheskikh Nauk* **176**, 664 (2006).
- [9] M. Y. Volkov and K. M. Salikhov, *Applied Magnetic Resonance* **41**, 145 (2011).
- [10] I. K. Kominis, *Physical Review E* **80** (2009), 10.1103/physreve.80.056115.
- [11] J. Cai, G. G. Guerreschi, and H. J. Briegel, *Physical Review Letters* **104** (2010), 10.1103/physrevlett.104.220502.
- [12] E. M. Gauger, E. Rieper, J. J. L. Morton, S. C. Benjamin, and V. Vedral, *Physical Review Letters* **106** (2011), 10.1103/physrevlett.106.040503.
- [13] I. K. Kominis, *Physical Review E* **83** (2011), 10.1103/physreve.83.056118.
- [14] M. Tiersch and H. J. Briegel, *Philosophical Transactions of the Royal Society A: Mathematical, Physical and Engineering Sciences* **370**, 4517 (2012).
- [15] H. J. Hogben, T. Biskup, and P. J. Hore, *Physical Review Letters* **109** (2012), 10.1103/physrevlett.109.220501.
- [16] J. A. Pauls, Y. Zhang, G. P. Berman, and S. Kais, *Phys-*

- ical Review E **87** (2013), 10.1103/physreve.87.062704.
- [17] M. Kritsotakis and I. K. Kominis, *Physical Review E* **90** (2014), 10.1103/physreve.90.042719.
- [18] Y. Zhang, G. P. Berman, and S. Kais, *International Journal of Quantum Chemistry* **115**, 1327 (2015).
- [19] L.-S. Guo, B.-M. Xu, J. Zou, and B. Shao, *Scientific Reports* **7** (2017), 10.1038/s41598-017-06187-y.
- [20] K. M. Vitalis and I. K. Kominis, *Physical Review A* **95** (2017), 10.1103/physreve.95.032129.
- [21] K. Mouloudakis and I. K. Kominis, *Physical Review E* **95** (2017), 10.1103/physreve.95.022413.
- [22] I. K. Kominis, *Physical Review Research* **2** (2020), 10.1103/physrevresearch.2.023206.
- [23] T. P. Fay, L. P. Lindoy, D. E. Manolopoulos, and P. J. Hore, *Faraday Discussions* **221**, 77 (2020).
- [24] V. A. Bagryansky, V. I. Borovkov, and Y. N. Molin, *Russian Chemical Reviews* **76**, 493 (2007).
- [25] Y. N. Molin, *Mendeleev Communications* **14**, 85 (2004).
- [26] N. M. Yu, *Bulletin of the Korean Chemical Society* **20**, 7 (1999).
- [27] B. Brocklehurst, *Chemical Society Reviews* **31**, 301 (2002).
- [28] V. Bagryansky, K. Ivanov, V. Borovkov, N. Lukzen, and Y. N. Molin, *The Journal of chemical physics* **122**, 224503 (2005).
- [29] J. Jones and P. Hore, *Chemical Physics Letters* **488**, 90 (2010).
- [30] A. I. Shushin, *The Journal of Chemical Physics* **133**, 044505 (2010).
- [31] L. V. Il'ichov and S. V. Anishchik, arXiv preprint arXiv:1003.1793 (2010).
- [32] K. L. Ivanov, M. V. Petrova, N. N. Lukzen, and K. Maeda, *The Journal of Physical Chemistry A* **114**, 9447 (2010).
- [33] P. Purto, *Chemical Physics Letters* **496**, 335 (2010).
- [34] J. Jones, K. Maeda, and P. Hore, *Chemical Physics Letters* **507**, 269 (2011).
- [35] I. K. Kominis, *Chemical Physics Letters* **508**, 182 (2011).
- [36] J. Jones, K. Maeda, U. Steiner, and P. Hore, *Chemical Physics Letters* **508**, 184 (2011).
- [37] M. Tiersch, U. E. Steiner, S. Popescu, and H. J. Briegel, *The Journal of Physical Chemistry A* **116**, 4020 (2012).
- [38] A. Dellis and I. Kominis, *Chemical Physics Letters* **543**, 170 (2012).
- [39] V. Bagryansky, V. Borovkov, and Y. Molin, *Chemical Physics Letters* **570**, 141 (2013).
- [40] (2019), 20-qubit backend: IBM Q team, "IBM Q 20 Almaden backend specification V1.3.1," (2019).
- [41] M. M. Vyushkova, V. I. Borovkov, L. N. Shchegoleva, I. V. Beregovaya, V. A. Bagryansky, and Y. N. Molin, *Doklady Physical Chemistry* **420**, 125 (2008).
- [42] B. Brocklehurst, *J. Chem. Soc., Faraday Trans. 2* **72**, 1869 (1976).
- [43] V. Bagryansky, O. Usov, N. Lukzen, and Y. N. Molin, *Applied Magnetic Resonance* **12**, 505 (1997).
- [44] U. E. Steiner and T. Ulrich, *Chemical Reviews* **89**, 51 (1989).
- [45] J. Preskill, *California Institute of Technology* **16** (1998).
- [46] A. Fujiwara, *Physical Review A* **89** (2004), 10.1103/PhysRevA.70.012317.
- [47] G. H. Low and I. L. Chuang, *Physical review letters* **118**, 010501 (2017).
- [48] D. W. Berry, A. M. Childs, R. Cleve, R. Kothari, and R. D. Somma, *Physical review letters* **114**, 090502 (2015).
- [49] J. D. Whitfield, J. Biamonte, and A. Aspuru-Guzik, *Molecular Physics* **109**, 735 (2011).
- [50] R. Babbush, N. Wiebe, J. McClean, J. McClain, H. Neven, and G. K.-L. Chan, *Physical Review X* **8**, 011044 (2018).
- [51] J. T. Barreiro, M. Müller, P. Schindler, D. Nigg, T. Monz, M. Chwalla, M. Hennrich, C. F. Roos, P. Zoller, and R. Blatt, *Nature* **470**, 486 EP (2011), article.
- [52] L. Del Re, B. Rost, A. F. Kemper, and J. K. Freericks, *Phys. Rev. B* **102**, 125112 (2020).
- [53] D. C. McKay, C. J. Wood, S. Sheldon, J. M. Chow, and J. M. Gambetta, *Physical Review A* **96**, 022330 (2017).
- [54] H. Abraham, I. Y. Akhalwaya, G. Aleksandrowicz, T. Alexander, G. Alexandrowics, E. Arbel, A. Asfaw, C. Azaustre, P. Barkoutsos, G. Barron, L. Bello, Y. Ben-Haim, D. Bevenius, L. S. Bishop, S. Bosch, D. Bucher, CZ, F. Cabrera, P. Calpin, L. Capelluto, J. Carballo, G. Carrascal, A. Chen, C.-F. Chen, R. Chen, J. M. Chow, C. Claus, C. Clauss, A. J. Cross, A. W. Cross, J. Cruz-Benito, Cryoris, C. Culver, A. D. Córcoles-Gonzales, S. Dague, M. Dartiaillh, A. R. Davila, D. Ding, E. Dumitrescu, K. Dumon, I. Duran, P. Eendebak, D. Egger, M. Everitt, P. M. Fernández, A. Frisch, A. Fuhrer, I. GOULD, J. Gacon, Gadi, B. G. Gago, J. M. Gambetta, L. Garcia, S. Garion, Gawel-Kus, J. Gomez-Mosquera, S. de la Puente González, D. Greenberg, J. A. Gunnel, I. Haide, I. Hamamura, V. Havlicek, J. Hellmers, L. Herok, H. Horii, C. Howington, S. Hu, W. Hu, H. Imai, T. Imamichi, R. Iten, T. Itoko, A. Javadi-Abhari, Jessica, K. Johns, N. Kanazawa, A. Karazeev, P. Kassebaum, A. Kovyshin, V. Krishnan, K. Krsulich, G. Kus, R. LaRose, R. Lambert, J. Latone, S. Lawrence, D. Liu, P. Liu, P. B. Z. Mac, Y. Maeng, A. Malyshev, J. Marecek, M. Marques, D. Mathews, A. Matsuo, D. T. McClure, C. McGarry, D. McKay, S. Meesala, A. Mezza-capo, R. Midha, Z. Mineev, M. D. Mooring, R. Morales, N. Moran, P. Murali, J. Müggenburg, D. Nadlinger, G. Nannicini, P. Nation, Y. Naveh, Nick-Singstock, P. Niroula, H. Norlen, L. J. O'Riordan, P. Ollitrault, S. Oud, D. Padilha, H. Paik, S. Perriello, A. Phan, M. Pistoia, A. Pozas-iKerstjens, V. Prutyaynov, J. Pérez, Quintiii, R. Raymond, R. M.-C. Redondo, M. Reuter, D. M. Rodríguez, M. Ryu, M. Sandberg, N. Sathaye, B. Schmitt, C. Schnabel, T. L. Scholten, E. Schoute, I. F. Sertage, N. Shammah, Y. Shi, A. Silva, Y. Siraichi, S. Sivarajah, J. A. Smolin, M. Soeken, D. Steenzen, M. Stypulkoski, H. Takahashi, C. Taylor, P. Taylour, S. Thomas, M. Tillet, M. Tod, E. de la Torre, K. Trabing, M. Treinish, TrishaPe, W. Turner, Y. Vaknin, C. R. Valcarce, F. Varchon, D. Vogt-Lee, C. Vuillot, J. Weaver, R. Wiczorek, J. A. Wildstrom, R. Wille, E. Winston, J. J. Woehr, S. Woerner, R. Woo, C. J. Wood, R. Wood, S. Wood, J. Wootton, D. Yeralin, J. Yu, L. Zdanski, Zoufal, anedumla, azulenhner, bcammorrison, brandhsn, dennis-liu 1, drholmie, elfrocampeador, fanizzamarco, gruu, kanejess, klinvill, lerongil, ma5x, merav aharoni, mrossinek, ordmoj, strickromon, tigerjack, yang.luh, and yotamvakninibm, "Qiskit: An open-source framework for quantum computing," (2019).
- [55] P. Jurcevic, A. Javadi-Abhari, L. S. Bishop, I. Lauer, D. F. Bogorin, M. Brink, L. Capelluto, O. Günlük, T. Itoko, N. Kanazawa, *et al.*, arXiv preprint arXiv:2008.08571 (2020).
- [56] N. Sundaresan, I. Lauer, E. Pritchett, E. Magesan,

- P. Jurcevic, and J. M. Gambetta, arXiv preprint arXiv:2007.02925 (2020).
- [57] Y. Wang, M. Um, J. Zhang, S. An, M. Lyu, J.-N. Zhang, L.-M. Duan, D. Yum, and K. Kim, *Nature Photonics* **11**, 646 (2017).
- [58] A. Kandala, K. Temme, A. D. Córcoles, A. Mezzacapo, J. M. Chow, and J. M. Gambetta, *Nature* **567**, 491 (2019).
- [59] Y. Molin and K. Salikhov, *Chemical Physics Letters* **211**, 484 (1993).
- [60] P. Krantz, M. Kjaergaard, F. Yan, T. P. Orlando, S. Gustavsson, and W. D. Oliver, *Applied Physics Reviews* **6**, 021318 (2019).
- [61] O. M. Usov, D. V. Stass, B. M. Tadjikov, and Y. N. Molin, *The Journal of Physical Chemistry A* **101**, 7711 (1997).
- [62] A. Veselov, V. Melekhov, O. Anisimov, and Y. N. Molin, *CPL* **136**, 263 (1987).
- [63] V. Bagryansky, “Private communication,” (2020).